Seizures and enhanced cortical GABAergic inhibition in two mouse models of human autosomal dominant nocturnal frontal lobe epilepsy

Alwin Klaassen*, Joseph Glykys*, Jamie Maguire†, Cesar Labarca‡, Istvan Mody†, and Jim Boulter§¶

§Department of Psychiatry and Biobehavioral Sciences, Hatos Research Center for Neuropharmacology, Brain Research and Molecular Biology Institutes, and *Graduate Interdepartmental Program in Neuroscience, 675 Charles Young Drive South, University of California, Los Angeles, CA 90095; †Department of Neurology, 655 Charles Young Drive South, University of California, Los Angeles, CA 90095; and ‡Division of Biology, California Institute of Technology, Pasadena, CA 91125

Communicated by Stephen F. Heinemann, The Salk Institute for Biological Studies, San Diego, CA, September 18, 2006 (received for review May 30, 2006)

Selected mutations in the human $\alpha4$ or $\beta2$ neuronal nicotinic acetylcholine receptor subunit genes cosegregate with a partial epilepsy syndrome known as autosomal dominant nocturnal frontal lobe epilepsy (ADNFLE). To examine possible mechanisms underlying this inherited epilepsy, we engineered two ADNFLE mutations (*Chrna4*^{S252F} and *Chrna4*$^{+L264}$) in mice. Heterozygous ADNFLE mutant mice show persistent, abnormal cortical electroencephalograms with prominent delta and theta frequencies, exhibit frequent spontaneous seizures, and show an increased sensitivity to the proconvulsant action of nicotine. Relative to WT, electrophysiological recordings from ADNFLE mouse layer II/III cortical pyramidal cells reveal a >20-fold increase in nicotine-evoked inhibitory postsynaptic currents with no effect on excitatory postsynaptic currents. i.p. injection of a subthreshold dose of picrotoxin, a use-dependent γ-aminobutyric acid receptor antagonist, reduces cortical electroencephalogram delta power and transiently inhibits spontaneous seizure activity in ADNFLE mutant mice. Our studies suggest that the mechanism underlying ADNFLE seizures may involve inhibitory synchronization of cortical networks via activation of mutant $\alpha4$-containing nicotinic acetylcholine receptors located on the presynaptic terminals and somatodendritic compartments of cortical GABAergic interneurons.

cortex | GABAegic interneuron | nicotinic acetylcholine receptor

Epilepsy is a common neurological disorder affecting ≈1% of the population worldwide. Over the past decade, several idiopathic epilepsies have been identified that show single-gene inheritance. Autosomal dominant nocturnal frontal lobe epilepsy (ADNFLE) was the first idiopathic epilepsy for which specific mutations were described (1). Segregation and subsequent linkage analyses of ADNFLE families led to the assignment of candidate genetic loci and ultimately to the identification of specific mutations. Two of the three loci associated with this partial epilepsy (ENFL1, 20q13.3 and ENFL3, 1p21) map to neuronal nicotinic acetylcholine receptor (nAChR) subunit genes $\alpha4$ and $\beta2$ (*CHRN*B2), respectively. A candidate gene for the third locus (ENFL2, 15q24) has not been identified. Considerable clinical and genetic data now provide a strong link between the ADNFLE syndrome and six mutations located within the pore-forming, second transmembrane domain of the $\alpha4$ (S252F, +L264, S256L, T265I) and $\beta2$ (V287L, V287M) nAChR subunits (2), as well as a single mutation located in the third transmembrane domain of the $\beta2$ subunit (I312M) (3).

In most patients with ADNFLE, seizure onset occurs during adolescence with symptoms persisting into adulthood. Affected individuals typically present without adverse neurological symptoms other than seizures, although several reports describe ADNFLE patients with a concomitant history of psychiatric problems (4, 5), cognitive deficits (3), or mental retardation (6). Clinical features of ADNFLE include clusters of brief seizures that initiate during non-rapid eye movement (NREM) sleep. Ictal and interictal electroencephalograms (EEGs) are often uninformative and clinical diagnosis is best achieved by using a combination of nocturnal video-polysomnography and genetic analyses (7). Whereas the frontal lobe origin, adolescent onset, and clusters of nocturnal, hyperkinetic motor seizures are signatures of this disorder, the ADNFLE seizure phenotype shows incomplete penetrance and can present with (6, 8) or without (4, 9) intra- and interfamilial variation in expressivity.

Given the similarities in clinical symptoms, it has been suggested that a common functional anomaly of mutant $\alpha4$- and $\beta2$-subunit-containing nAChRs underlies ADNFLE. However, studies in heterologous expression systems designed to discover a shared, altered property that might explain the neuronal network dysfunction underlying ADNFLE seizures have lead to both "gain-of-function" (10–12) and "loss-of-function" (8, 13, 14) models. The effect of stimulating nAChRs (mutant or otherwise) on cortical network activity is difficult to predict, hence, insight into the mechanism responsible for neuronal synchrony and epileptogenesis in ADNFLE must necessarily come from models that attempt to reconstitute the *in vivo* distribution and function of mutant nAChRs. To more fully understand the pathophysiology and mechanism underlying this epilepsy, we genetically engineered two mouse strains that harbor the ADNFLE *Chrna4*^{S252F} and *Chrna4*$^{+L264}$ mutant alleles. The characterization and validation of this mouse model of ADNFLE should provide an important tool with which to examine the molecular, cellular, and developmental basis for epileptogenesis.

Results

Heterozygous and homozygous ADNFLE mutant mouse strains are viable, show expected gender and Mendelian genotype ratios, express equal levels of WT and mutant $\alpha4$ transcripts, and exhibit no gross neuroanatomical abnormalities (Figs. 5–8, which are published as supporting information on the PNAS web site). However, relative to age and gender-matched WT littermates, all heterozygous *Chrna4*$^{S252F/wt}$ and *Chrna4*$^{+L264/wt}$ mice show abnormal EEGs, which are characterized by a marked increase in δ wave activity (0.5–4 Hz) (Fig. 1*a*). Similar results were observed with

Author contributions: A.K., J.G., and J.M. contributed equally to this work; A.K., J.G., J.M., I.M., and J.B. designed research; A.K., J.G., J.M., and J.B. performed research; A.K., J.G., J.M., C.L., I.M., and J.B. contributed new reagents/analytic tools; A.K., J.G., J.M., I.M., and J.B. analyzed data; and J.B. wrote the paper.

The authors declare no conflict of interest.

Freely available online through the PNAS open access option.

Abbreviations: ACh, acetylcholine; ACSF, artificial cerebrospinal fluid; EEG, electroencephalogram; mIPSC, miniature inhibitory postsynaptic current; nAChR, nicotinic ACh receptor; NREM, non-rapid eye movement; PTX, picrotoxin; sIPSC, spontaneous inhibitory postsynaptic current.

¶To whom correspondence should be addressed. E-mail: jboulter@ucla.edu.

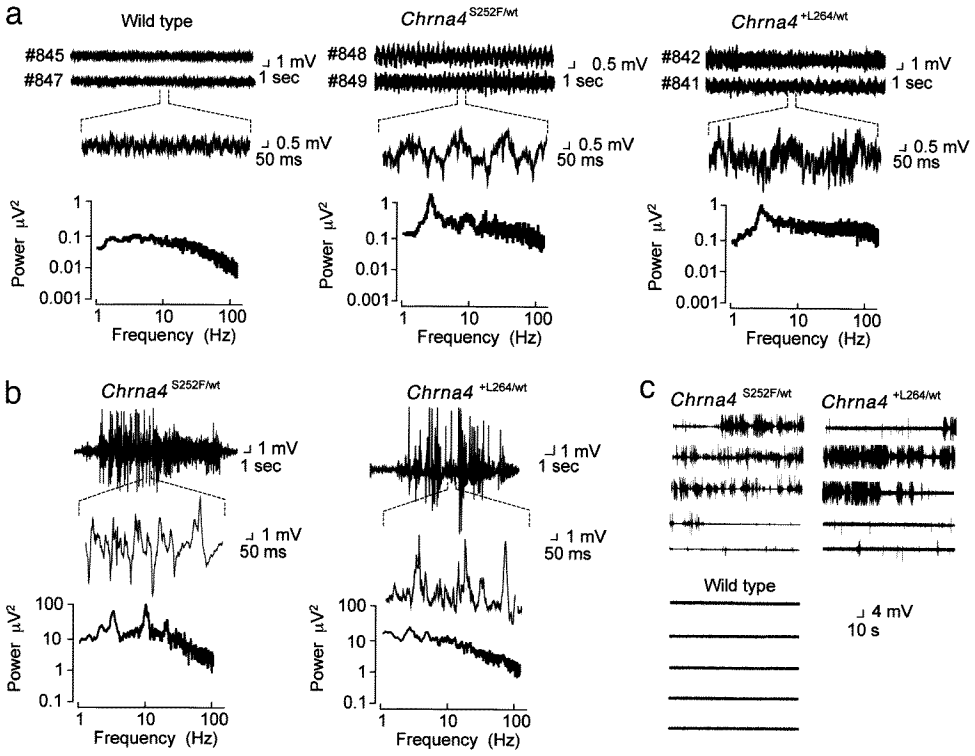

Fig. 1. Both *Chrna4*$^{S252F/wt}$ and *Chrna4*$^{+L264/wt}$ mice exhibit abnormal cortical EEGs and show spontaneous, repetitive EEG discharges with paroxysmal onset and sudden termination. (*a*) Relative to WT, fast Fourier transform analyses of recordings from awake *Chrna4*$^{S252F/wt}$ and *Chrna4*$^{+L264/wt}$ mice show a marked increase in δ (0.5–4 Hz) and, in the case of *Chrna4*$^{S252F/wt}$ mice, θ frequencies (4–8 Hz). (*b* and *c*) EEG recordings during spontaneous seizures in *Chrna4*$^{S252F/wt}$ and *Chrna4*$^{+L264/wt}$ mice. (*b*) Higher-resolution traces show complex patterns of spike and wave activity with high-amplitude, low-frequency power spectra in *Chrna4*$^{S252F/wt}$ mice, and a more asymmetric, diffuse pattern in *Chrna4*$^{+L264/wt}$ mice. (*c*) The traces show ≈15 min of continuous EEG data, including the periods immediately before and after paroxysmal discharges in *Chrna4*$^{S252F/wt}$ and *Chrna4*$^{+L264/wt}$ mice. Note pre- and postictal spiking in ADNFLE mutant mice and the sudden onset of clusters of high-amplitude spikes.

homozygous *Chrna4*$^{S252F/S252F}$ and *Chrna4*$^{+L264/+L264}$ mice (Fig. 9, which is published as supporting information on the PNAS web site). A considerable increase in θ wave activity (4–8 Hz) also is evident in the EEG patterns of *Chrna4*$^{S252F/wt}$ (Fig. 1*a*), *Chrna4*$^{S252F/S252F}$, and *Chrna4*$^{+L264/+L264}$ mice (Fig. 9*a*). Such abnormal EEGs were observed ≈50–80% of the time during every 4-hour recording epoch in *Chrna4*$^{S252F/wt}$ (n = 10) and *Chrna4*$^{+L264/wt}$ (n = 4) mice (Fig. 10, which is published as supporting information on the PNAS web site).

In addition to abnormal EEGs, heterozygous *Chrna4*$^{S252F/wt}$ and *Chrna4*$^{+L264/wt}$ mice exhibit recurrent spontaneous seizures, which are accompanied by high-amplitude, low-frequency cortical EEG activity (Fig. 1*b*). Seizure semiology ranges from brief periods (1–5 s) of behavioral arrest to extended periods (2–60 min) of rhythmic, jerking motion involving all extremities, loss of balance, and frequent falling to one side (Movie 1, which is published as supporting information on the PNAS web site). Fig. 1 *b* and *c* show sample EEGs obtained from subdural recording electrodes during spontaneous seizures of *Chrna4*$^{S252F/wt}$ (n = 10) and *Chrna4*$^{+L264/wt}$ (n = 4) mice. Such repetitive EEG discharges characterized by paroxysmal onset, sudden termination, and asymmetric rhythmic patterns of spiking activity were observed during 5.1 ± 3.6% of each 4-hour recording epoch in *Chrna4*$^{+L264/wt}$ mice and 22.0 ± 11.7% in *Chrna4*$^{S252F/wt}$ mice. Similar seizure activity was observed in homozygous *Chrna4*$^{S252F/S252F}$ and *Chrna4*$^{+L264/+L264}$ mice, which exhibited epileptiform activity 21.5 ± 5.4% and 5.7 ± 3.5% of the time, respectively (Fig. 10*b*).

Having established that heterozygous *Chrna4*$^{S252F/wt}$ and *Chrna4*$^{+L264/wt}$ mice exhibit spontaneous seizures, we sought to investigate the electrophysiological mechanism underlying epileptogenesis at the level of cortical circuits. Although α4-containing nAChRs are widely expressed in the vertebrate brain, altered cholinergic activation of neocortical and/or thalamocortical networks may play a central role in the generation of ADNFLE seizures as EEG recordings from ADNFLE patients suggest that seizures originate in the frontal lobe of the neocortex (7). Because synaptic activity in pyramidal cells is a major source of cortical EEG activity, we first examined the effect of ADNFLE mutations on the synaptic events of layer II/III pyramidal cells of the frontal cortex.

Whole-cell voltage-clamp recordings of spontaneous excitatory postsynaptic currents and spontaneous inhibitory postsynaptic currents (sIPSCs) were obtained from layer II/III pyramidal cells of WT and *Chrna4*$^{S252F/wt}$ mouse brain slices (Fig. 2). There were no significant differences between the excitatory or inhibitory synaptic events recorded under control conditions in WT and *Chrna4*$^{S52F/wt}$ mouse pyramidal cells (Tables 2 and 3, which are published as supporting information on the PNAS web site). We next examined whether activation of WT and ADNFLE mutant nAChRs by nicotine (1 μM) results in differential effects on synaptic currents. Regardless of genotype, nicotine had no effect on spontaneous excitatory postsynaptic current frequency, kinetics, or amplitude during 30-s recording periods sampled during drug perfusion ($P \geq 0.05$, paired and unpaired t test; Fig. 2 and Table 2). In marked contrast, the effect of nicotine on IPSCs was dramatically different between WT and ADNFLE mutant mice. In WT brain slices, nicotine had little effect on sIPSC frequency or kinetics (Fig. 2, $n = 6$; $P \geq 0.05$, paired t test; Table 3), whereas it significantly increased both frequency and amplitude of sIPSCs in *Chrna4*$^{S252F/wt}$ pyramidal cells (Fig. 2, n = 5; $P < 0.05$, paired t test; Table 3). To better resolve the

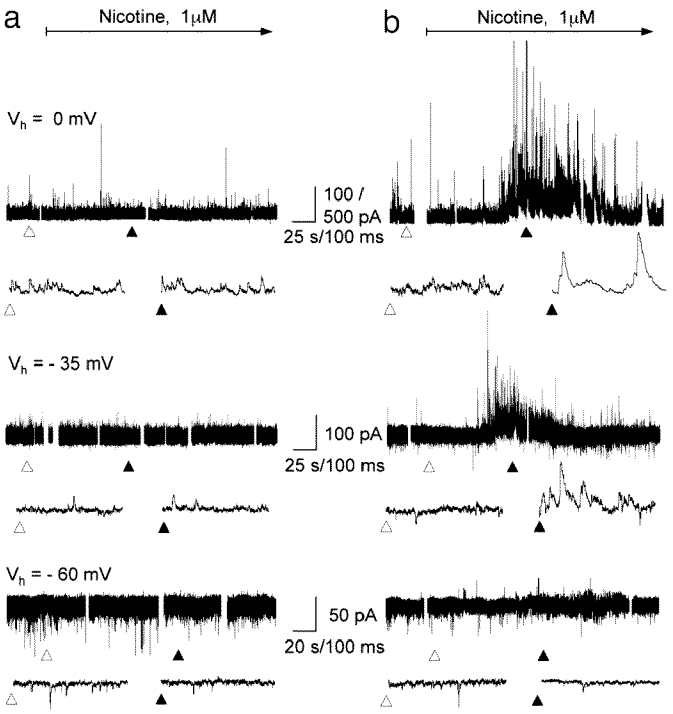

Fig. 2. Nicotine increases sIPSCs recorded from cortical layer II/III pyramidal cells without affecting spontaneous excitatory postsynaptic currents. Voltage clamp recordings were obtained from WT (*a*) and *Chrna4*$^{S252F/wt}$ cortical layer II/III pyramidal (*b*) cells immediately before and during perfusion of ACSF containing nicotine (1 μM, shown by a solid bar). In *Chrna4*$^{S252F/wt}$ slices, nicotine induced a net increase in pyramidal cell inhibitory I_{mean} (V_h = 0 mV) of 23.4 ± 5.0-fold (n = 6), whereas for WT, the I_{mean} ratio was 2.5 ± 0.4-fold (n = 9). Gaps in the current traces indicate times at which membrane seal tests were performed, and expanded traces are shown for periods corresponding to perfusion with ACSF alone (△) or ACSF plus nicotine (▲).

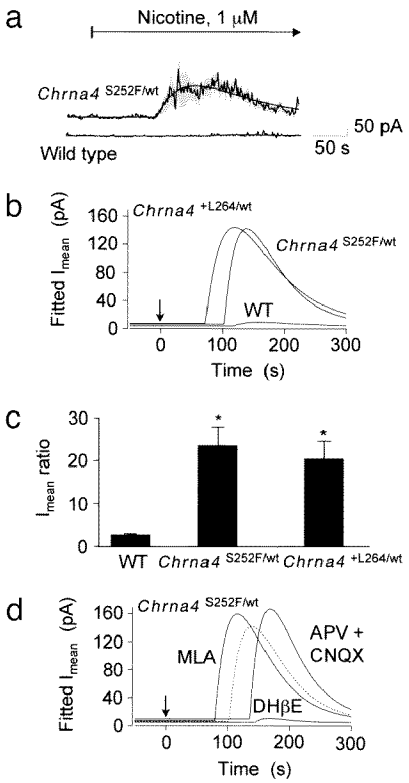

Fig. 3. The pharmacology and kinetics of nicotine-enhanced, cortical pyramidal cell sIPSCs are similar in brain slices prepared from both *Chrna4*$^{S252F/wt}$ and *Chrna4*$^{+L264/wt}$ mice. (*a*) Recordings from WT (lower trace; n = 8) and *Chrna4*$^{S252F/wt}$ (upper trace; n = 6) cortical layer II/III pyramidal cells immediately before and during perfusion of ACSF containing nicotine. Averages of the recordings were fit to an α function (smooth solid line), with the shaded area corresponding to the SEM. (*b*) The fitted sIPSC mean values (I_{mean}, baseline subtracted) in WT (n = 8), *Chrna4*$^{S252F/wt}$ (n = 6), and *Chrna4*$^{+L264/wt}$ (n = 5) cortical pyramidal cells before and during perfusion of ACSF containing nicotine (1 μM at time 0 s, arrow). (*c*) The normalized sIPSC ratios (peak current in the presence of 1 μM nicotine divided by control responses) for WT (n = 8), *Chrna4*$^{S252F/wt}$ (n = 6), and *Chrna4*$^{+L264/wt}$ (n = 5) cortical pyramidal cells. *, $P <$ 0.05, one-way ANOVA. (*d*) The fitted sIPSC mean values (I_{mean}, baseline subtracted) in *Chrna4*$^{S252F/wt}$ cortical pyramidal cells after perfusion of nicotine (1 μM at time 0 s, arrow) in the presence of 50 nM methyllycaconitine (MLA) (n = 6), 10 μM dihydro-β-erythroidine (DHβE) (n = 3), or a mixture of 10 μM 6-cyano-7-nitroquinoxaline-2′-dione (CNQX) and 25 μM APV (n = 4). The dotted line represents the response to nicotine alone.

compound effect of nicotine on the frequency, amplitude, and kinetics of sIPSCs, we measured the mean inhibitory current (I_{mcan}, see *Methods*) and calculated the effect of nicotine as the ratio of I_{mcan} measured before and after its perfusion (Fig. 3*a*). Fitting an α-function to the inhibitory I_{mcan} allowed us to determine the latency and decay of the nicotine effect, and these parameters are approximately proportional to the sensitivity and desensitization of the nicotine responses, respectively.

On average, the effect of nicotine (1 μM) on the inhibitory I_{mcan} (V_h = 0 mV) was a 23.4 ± 5.0-fold (n = 6) increase over baseline in *Chrna4*$^{S252F/wt}$ pyramidal cells. A similar treatment in WT pyramidal cells increased inhibitory I_{mcan} only 2.5 ± 0.4-fold (n = 8; $P < 0.05$, one-way ANOVA; Fig. 3 *a–c*). Nicotine also caused large increases in I_{mcan} in *Chrna4*$^{+L264/wt}$ pyramidal cells (20.1 ± 5.6-fold; $P < 0.05$, one-way ANOVA; n = 5, Fig. 3*b*). The nicotine effects on I_{mcan} showed similar decay across genotypes (τ, Fig. 3 *b* and *d*). The effect of nicotine on I_{mcan} did not change when glutamate receptors were blocked by D-2-amino-5-phosphonovaleric acid (25 μM) and 6-cyano-7-nitroquinoxaline-2′-dione (CNQX) (10 μM) (18.2 ± 2.3-fold increase, n = 4; $P >$ 0.05, unpaired t test; Fig. 3*d*), indicating that nicotine has little effect on the excitatory drive onto the interneurons. We also tested the effects of antagonists to ensure that the effects of nicotine were mediated by α4-subunit-containing nAChRs. The nicotine-induced inhibition was insensitive to an antagonist of α7-subunit-containing nAChRs [methyllycaconitine (MLA), 50 nM, n = 6, Fig. 3*d*]. In contrast, perfusion of the α4β2 nAChR subtype-selective antagonist dihydro-β-erythroidine (DHβE) (10 μM, n = 3) resulted in ≥90% decrease in the effect of nicotine on inhibitory I_{mcan} (2.20 ± 0.83 vs. 23.4 ± 5.0, $P < 0.05$, t test assuming unequal variances; Fig. 3*d*).

Based on combined electrophysiological (15) and molecular studies (16), the observed increase in inhibitory I_{mcan} is very likely a result of an enhanced nicotine-evoked GABA release from *Chrna4*$^{S252F/wt}$ or *Chrna4*$^{+L264/wt}$-expressing cortical interneurons that form synapses on the somata, axon initial segments, or dendrites of pyramidal cells. To determine whether nicotine acts on α4-subunit-containing nAChRs located on GABAergic interneuron terminals, we measured its effect on miniature IPSCs (mIPSCs) recorded in the absence of presynaptic Ca^{2+} entry by blocking action potentials with tetrodotoxin (TTX) and voltage-gated Ca^{2+} channels with cadmium. Perfusion of WT brain slices with TTX (0.5 μM) and $CdCl_2$ (50 μM) significantly decreased the frequency (≈27%) and amplitude (≈34%) of pyramidal cell IPSCs indicating that a large fraction of sIPSCs are mediated by Ca^{2+} entry into GABAergic terminals (data not shown). The mIPSCs of WT and *Chrna4*$^{S252F/wt}$ pyramidal cells were not significantly different ($P > 0.05$, unpaired t test, Table 1), and addition of nicotine (1 μM) did not alter mIPSCs

Table 1. Nicotine increases frequency, amplitude, and alters response kinetics of mIPSCs in pyramidal cell neurons of *Chrna4*$^{S252F/wt}$ mice

	WT		*Chrna4*$^{S252F/wt}$	
Measurement	Control	Nicotine	Control	Nicotine
Frequency, per sec	20.1 ± 5.0	18.4 ± 4.3	16.8 ± 1.4	29.0 ± 2.8*
Peak amplitude, pA	15.2 ± 1.5	13.0 ± 1.4	16.1 ± 0.8	19.5 ± 0.9*
Rise time 10–90, ms	0.84 ± 0.05	1.03 ± 0.07	0.86 ± 0.05	0.89 ± 0.06
τ_{decay}, ms	6.83 ± 0.38	7.08 ± 0.36	6.72 ± 0.13	7.43 ± 0.26*

Whole-cell voltage clamp recordings (V_h = 0 mV) were obtained from frontal cortex layer II/III pyramidal cells in the presence of APV (25 μM), CNQX (10 μM), $CdCl_2$ (50 μM), and TTX (0.5 μM). Events were detected and analyzed in 60-s segments. Values represent the mean ± SEM. Comparisons were made between nicotine-treated (1 μM) WT (n = 4) and *Chrna4*$^{S252F/wt}$ (n = 7) brain slices. Values with asterisks represent $P < 0.05$ by using a paired t test. No statistical differences were found between control values of both genotypes ($P > 0.05$, unpaired t test).

frequency and kinetics in the WT ($P > 0.05$, paired t test, n = 4; Table 1). Even when presynaptic voltage-gated Na^+ and Ca^{2+} channels were blocked, nicotine significantly increased the amplitude (17%) and frequency (42%) of mIPSCs in *Chrna4*$^{S252F/wt}$ brain slices ($P < 0.05$, paired t test; n = 7; Table 1). The combined effect of nicotine on mIPSC frequency and amplitude resulted in an increased inhibitory I_{mean} of 3.38 ± 0.57-fold (n = 8) in the absence of any voltage-gated Na^+ and Ca^{2+} entry into the terminals. Thus, a considerable fraction of ADNFLE mutant α4-subunit-containing nAChRs are located on presynaptic terminals of cortical GABAergic interneurons and elevate presynaptic Ca^{2+} levels.

To explore the relationship between increased GABA-mediated IPSCs, abnormal cortical EEGs, and seizure activity in ADNFLE mutant mice, we examined the effect of picrotoxin (PTX), a use-dependent antagonist of $GABA_A$ receptors, on the EEG and spontaneous seizures in *Chrna4*$^{S252F/wt}$ mice. The data in Fig. 4 reveal that in WT mice, i.p. injection of low-dose PTX (0.1 mg/kg) has little effect on the cortical EEG, relative δ power, and percentage of time exhibiting δ wave activity (Fig. 4 *a*, *c*, and *d*) and shows no proconvulsant activity (Fig. 4*e*). However, in *Chrna4*$^{S252F/wt}$ mice, this subthreshold dose "normalizes" the baseline EEG (Fig. 4*b*), decreases the relative power and time-expressing δ wave activity (Fig. 4 *c* and *d*), and completely inhibits spontaneous seizure activity (Fig. 4*e*).

Discussion

Whereas genetic factors contribute to ≈40% of all human epilepsies, <30 idiopathic epilepsy syndromes show a monogenic mode of inheritance and, of those, only 12 disorders have been associated with a specific genetic locus (17). Here, we report two murine models of a human familial channelopathy linked to epilepsy. *In vivo*, the *Chrna4*^{S252F} and *Chrna4*$^{+L264}$ ADNFLE mutations both produce abnormal cortical EEG patterns, interictal spiking, and recurrent seizure activity in mice. The interictal spiking and spontaneous seizures seen in both *Chrna4*$^{S252F/wt}$ and

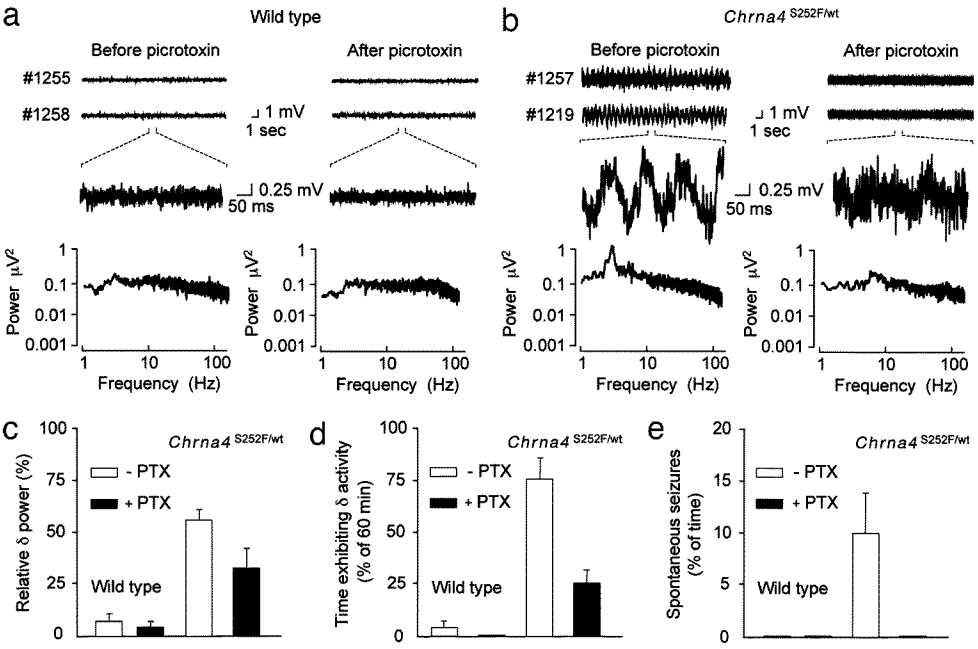

Fig. 4. *Chrna4*$^{S252F/wt}$ mice have abnormal cortical EEGs with persistent δ (0.5–4 Hz) activity, which is decreased by low-dose PTX. (*a*) WT EEGs do not significantly differ between pre- and post-PTX (0.1 mg/kg, i.p.) treatment. (*a* and *b*) FFT analyses of baseline recordings from WT (n = 6) (*a*) and *Chrna4*$^{S252F/wt}$ (n = 6) (*b*) mice illustrate the increase in δ power in *Chrna4*$^{S252F/wt}$ mice. FFT analysis also demonstrates the decrease in δ activity in *Chrna4*$^{S252F/wt}$ mice (n = 6) after treatment with PTX. PTX did not have an effect on the fast Fourier transform in WT mice (n = 6). (*c*) Compared with untreated controls, the relative contribution of δ activity is decreased after administration of PTX in *Chrna4*$^{S252F/wt}$ mice, with no significant difference seen in WT mice. (*d*) In addition to a decrease in power, the amount of time exhibiting δ wave activity was decreased in the 60-min period after PTX administration compared with the 60-min period immediately before PTX administration. Picrotoxin did not have a significant effect on the amount of time WT mice exhibited δ activity. (*e*) Low-dose PTX completely eliminates spontaneous seizures in *Chrna4*$^{S252F/wt}$ mice during the 60 min immediately after PTX injection.

Chrna4$^{+L264/wt}$ mice argue that these mutations are sufficient to cause ADNFLE in humans. In addition, heterozygous ADNFLE mice are considerably more sensitive to nicotine-induced seizures, show shorter latencies to seizure onset, and exhibit longer seizure durations than their WT littermates (Fig. 11, which is published as supporting information on the PNAS web site). Together with the marked stimulation by nicotine of pyramidal cell sIPSCs in *Chrna4*$^{S252F/wt}$ and *Chrna4*$^{+L264/wt}$ mice, our results suggest that ADNFLE seizure etiology and altered cortical EEG patterns may involve an increased response to acetylcholine.

Cholinergic afferents, which arise principally from the basal forebrain, innervate cholinoceptive neurons in all layers of the rodent frontal cortex and are especially prominent in layers II and III of the human cortex. Whereas rodent cortical layer II/III and V pyramidal neurons are not directly depolarized by nicotinic cholinergic agonists (16, 18, 19), selected subtypes of cortical interneurons express functional nAChRs assembled from $\alpha4$ and $\beta2$ subunits (with or without $\alpha5$) or $\alpha7$ subunits (16, 20). Inhibitory interneurons release GABA and have been implicated in nicotine-induced hippocampal seizures (21), as well as in models of cortical or hippocampal pathophysiology that result from nAChR activation, modulation of GABAergic tone, and subsequent inhibition or disinhibition of neuronal networks (15). It remains to be determined which subclass of cortical interneurons is responsible for the increased GABAergic drive onto layer II/III pyramidal cells. In rats, >96% of layer I interneurons express both $\alpha4\beta2$ and $\alpha7$ nAChR subtypes. However, it's unlikely that they play a direct role as nicotinic stimulation of layer I interneurons leads to an action potential-dependent increase in layer II/III interneuron sIPSC frequency, with no effect on layer II/III pyramidal cells (20). In layer II/III, $\alpha4\beta2$ nAChRs (with or without $\alpha5$) are found in a high percentage of regular (63%) and irregular-spiking (77%) interneurons, the majority of which (≈70%) coexpress vasoactive intestinal peptide and cholecystokinin (16). Such interneurons innervate adjacent pyramidal cells and are candidates for the nicotine-evoked increase in inhibition. Layer V low-threshold spiking interneurons, whose axonal arbors project upwards to layers II/III, also express nAChRs and could likewise contribute to the nicotine-enhanced sIPSC frequency (22). Ultimately, the use of paired recordings and detailed electrophysiological and anatomical studies should permit the identification of interneurons involved in the altered effects of acetylcholine (ACh).

As described for a variety of nocturnal epilepsy syndromes, ADNFLE seizures initiate exclusively or predominantly during NREM sleep (23). Moreover, in patients with partial epilepsies, NREM sleep (notably stage 2) potentiates, whereas REM sleep inhibits, interictal epileptiform discharges and propagation of focal seizures (24). At this time, we do not know the relationship between sleep-wake state and seizure onset in ADNFLE mice. Unfortunately, vigilance and sleep-staging algorithms heavily rely on EEG patterns to distinguish periods of wakefulness from REM and NREM sleep. Hence, the nearly continuous, abnormal cortical δ and θ activities seen in *Chrna4*$^{S252F/wt}$ and *Chrna4*$^{+L264/wt}$ ADNFLE mice confound analyses that would unequivocally establish a temporal relationship between slow wave sleep, onset of paroxysmal EEG discharges, and seizures. Establishing whether aberrant signaling within corticothalamic circuits contributes to epileptogenesis in ADNFLE and documenting the precise effect(s) of mutant $\alpha4$-subunit-containing nAChRs on network dynamics *in vivo* will require additional electrophysiological experiments.

Rather than demonstrating a failure of GABAergic inhibition in ADNFLE mice, our EEG and electrophysiological data are consistent with a model of epileptogenesis in which ACh significantly enhances cortical GABAergic transmission. An essential feature of our model (see Fig. 12, which is published as supporting information on the PNAS web site) is that asynchronously firing layer II/III pyramidal cells will be synchronized after recovery from a large GABAergic inhibition triggered by cholinergic activation of mutant nAChRs. The effect of PTX on cortical EEG and spontaneous seizure activity suggests that activation of $GABA_A$ receptors *per se* could lead to increased network synchrony and, thereby, contribute to ictogenesis in this murine model of ADNFLE. The idea of establishing neuronal synchrony via inhibition has substantial experimental support. For example, two hippocampal pyramidal cells connected to the same GABAergic interneuron readily synchronize their firing after recovering from the inhibition evoked by the interneuron (25). Also, in the hippocampus, ACh-dependent activation of interneurons produces inhibition of pyramidal cells followed by rebound spiking (26), and endogenous cortical ACh recently has been shown to enhance synchronized interneuron activity via activation of $\alpha4\beta2$ nAChRs (27). Importantly, in human focal cortical dysplasia tissue *in vitro* ictal activity is initiated via a synchronization mechanism that requires sustained activation of $GABA_A$ receptors (28). We propose, then, that an ACh-dependent sudden increase in GABAergic inhibition contributes to epileptogenesis through inhibitory resetting of synchronization. Possible alternative GABA-mediated mechanisms include direct excitatory effects of axo-axonic interneurons on layer II/III pyramidal cells (29) or pyramidal cell depolarization after intense $GABA_A$ receptor activation and changes in the GABA reversal potential (30).

In summary, our data show that both ADNFLE *Chrna4*^{S252F} and *Chrna4*$^{+L264}$ mutations are dominant and cause abnormal cortical EEGs, interictal spiking, and recurrent seizures in heterozygous mice harboring either of these mutations. The ameliorative effect of low-dose PTX on cortical EEG patterns and suppression of spontaneous seizures in *Chrna4*$^{S252F/wt}$ mice provides compelling evidence for enhanced GABAergic function in ADNFLE. Although many details of epileptogenesis, including the possible involvement of noncortical neuronal circuits, remain to be examined in this mouse model, it seems clear that a number of important and intriguing questions related to ANFLE now can be addressed (2). ADNFLE mutations change the physiology of the brain in ways that allow it to function normally most of the time, but also render it capable of recurrent seizures. Future cellular and systems-level analyses of mutant and WT mice should help identify all possible causative factors and clarify the pathophysiological mechanisms underlying the complete ADNFLE syndrome.

Experimental Procedures

Genetic Engineering of ADNFLE Mutant Mice. Genetic engineering of the ADNFLE mice is described in Fig. 5. All experiments were carried out under protocols approved by the University of California, Los Angeles Chancellor's Animal Research Committee. Mutant mice and other materials prepared during this study may be obtained upon request.

Electroencephalogram Recordings. A subdural cortical EEG recording electrode was placed under the skull (2.8 mm anterior to bregma, 1.5 mm lateral to the midline) of age-matched, adult male ($P > 90$) mice, and the electrode was fixed to the skull by using dental cement. EEG recordings (band-pass-filtered between 0.1 and 200 Hz, 8-pole Bessel; Frequency Devices, Haverhill, MA) were acquired for 4–8 h daily for up to 2 weeks and were sampled at 1 kHz by using an in-house LabView-based (National Instruments, Austin, TX) analysis program. Electrographic seizure events were defined as changes in the amplitude and frequency of the EEG activity, and the software measured their duration. Seizure susceptibility consisted of cumulative time seizing expressed as a percentage of the total recording time and the average duration of individual electrographic events. The percentage of time seizing was calculated as the cumulative

time of all seizure activity during the recording period divided by the total time of the recording period. The durations of individual electrographic events were measured between the start of the repetitive EEG pattern and the return of the EEG spectrum to baseline. PTX (0.1 mg/kg, i.p.) was administered after 60 min of baseline EEG recording and continued for 60 min after PTX administration. EEGs were compared between the 60 min pre-PTX administration and the 1-h post-PTX administration only. Statistical analysis was determined by using ANOVA.

Brain Slice Preparation, Electrophysiological Recordings, and Data Acquisition. Adult male mice (2–4 months old) were anesthetized with halothane, and the brain was removed and placed in ice-cold artificial cerebrospinal fluid (ACSF) containing 126 mM NaCl, 2.5 mM KCl, 2 mM $CaCl_2$, 2 mM $MgCl_2$, 1.25 mM NaH_2PO_4, 26 mM $NaHCO_3$, and 10 mM D-glucose (pH 7.3–7.4) when aerated with 95% O_2 and 5% CO_2. Frontal lobe coronal slices, 350 μm thick, were cut with a vibratome in ACSF containing 3 mM kynurenic acid. Slices were stored in ACSF in an interface chamber at 32°C for at least 1 h before being transferred to the recording chamber. Frontal cortex layer II/III pyramidal cells were identified visually by using video microscopy and recorded with an Axopatch 200B amplifier (Axon Instruments, Foster City, CA). Microelectrodes (1–3 MΩ) contained 140 mM cesium-methylsulfonate, 10 mM Hepes, 0.2 mM EGTA, 5 mM NaCl, 2 mM MgATP, 0.2 mM NaGTP (≈271 mOsm, pH ≈ 7.29). Series resistance and whole-cell capacitance were estimated from fast transients evoked by a 5 mV voltage command step by using a lag value of 7 μs and then compensated to 70–80%. Recordings were discontinued if series resistance increased by >25% through an experiment or if it reached ≥20 MΩ at any time during the experiment. All recordings were low-pass-filtered at 3 KHz (8-pole Bessel), digitized online at 10 KHz, and stored on videotape. Data were acquired, and spontaneous inhibitory and excitatory events were detected by using custom-written LabView-based software. All events were detected in 30–60 sec segments. Event frequency, peak amplitude, 10–90% rise time, and weighted decay time constant (τ_{dccay}) values were measured. Statistical significance was determined by using the *t* test (paired or unpaired assuming unequal variances) or by ANOVA with a Tukey's HSD post hoc test when the means of more than two groups were compared. The level of significance was set to $P < 0.05$.

Effect of Nicotine on Mean Inhibitory Current (I_{mean}). I_{mcan} was determined by using a macro running under IGOR Pro version 5.02 (WaveMetrics, Lake Oswego, OR). Briefly, the entire digitized recording was loaded, and seal tests were deleted. An all-point amplitude histogram was plotted for every 50,000 points (5 s) and smoothed, obtaining a distribution skewed in the direction of synaptic events. A Gaussian was fit to the part of the distribution that was not skewed (representing the baseline current and its noise), and the peak of this Gaussian was taken as the mean baseline current for the epoch. All baseline mean values were plotted, and linear trends were subtracted to normalize the mean baseline current to 0 pA. After baseline normalization, the cumulative sum of 10,000 data points (1 s) was calculated and divided by the number of points in that segment of time. Points on either side of the baseline (baseline noise) summed to 0, whereas anything above or below baseline summed to yield I_{mcan}. An α function was fitted to I_{mcan} obtaining the peak, latency, and decay of the nicotine effect in every cell. The equation used was as follows: $I_{mcan}(t) = A \times [(t - t_o)/\tau] \times \exp[1 - (t - t_o)/\tau] + y$, where A is the peak amplitude, t_o is the latency, τ is the decay, and y is the control base line. The I_{mcan} ratio was determined by dividing the peak amplitude of I_{mcan} during the nicotine effect by the I_{mcan} recorded before perfusion of nicotine.

This work was supported by a National Institute of Neurological Disorders and Stroke Molecular and Cellular Neuroscience training grant (to A.K.), a UCLA Gonda Fellowship (to J.G.), a Stein-Oppenheimer Endowment Award (to J.B.), and National Institute of Neurological Disorders and Stroke Grants NS02808 and NS30549 (to I.M.) and NS050419 (to J.B.). I.M. and J.B. acknowledge the support of the Coelho Endowment and the Milken Family Medical Foundation, respectively.

1. Phillips HA, Scheffer IE, Berkovic SF, Hollway GE, Sutherland GR, Mulley JC (1995) *Nat Genet* 10:117–118.
2. Sutor B, Zolles G (2001) *Pflügers Arch* 442:642–651.
3. Bertrand D, Elmslie F, Hughes E, Trounce J, Sander T, Bertrand S, Steinlein OK (2005) *Neurobiol Dis* 20:799–804.
4. McLellan A, Phillips HA, Rittey C, Kirkpatrick M, Mulley JC, Goudie D, Stephenson JB, Tolmie J, Scheffer IE, Berkovic SF, Zuberi SM (2003) *Epilepsia* 44:613–617.
5. Magnusson A, Stordal E, Brodtkorb E, Steinlein O (2003) *Psychiatr Genet* 13:91–95.
6. Cho YW, Motamedi GK, Laufenberg I, Sohn SI, Lim JG, Lee H, Yi SD, Lee JH, Kim DK, Reba R, *et al.* (2003) *Arch Neurol* 60:1625–1632.
7. Oldani A, Zucconi M, Asselta R, Modugno M, Bonati MT, Dalpra L, Malcovati M, Tenchini ML, Smirne S, Ferini-Strambi L (1998) *Brain* 121:205–223.
8. Steinlein OK, Magnusson A, Stoodt J, Bertrand S, Weiland S, Berkovic SF, Nakken KO, Propping P, Bertrand D (1997) *Hum Mol Genet* 6:943–947.
9. Scheffer IE, Bhatia KP, Lopes-Cendes I, Fish DR, Marsden CD, Andermann E, Andermann F, Desbiens R, Keene D, Cendes F, *et al.* (1995) *Brain* 118:61–73.
10. De Fusco M, Becchetti A, Patrignani A, Annesi G, Gambardella A, Quattrone A, Ballabio A, Wanke E, Casari G (2000) *Nat Genet* 26:275–276.
11. Bertrand D, Picard F, Le Hellard S, Weiland S, Favre I, Phillips H, Bertrand S, Berkovic SF, Malafosse A, Mulley J (2002) *Epilepsia* 43(Suppl 5):112–122.
12. Leniger T, Kananura C, Hufnagel A, Bertrand S, Bertrand D, Steinlein OK (2003) *Epilepsia* 44:981–985.
13. Kuryatov A, Gerzanich V, Nelson M, Olale F, Lindstrom J (1997) *J Neurosci* 17:9035–9047.
14. Bertrand S, Weiland S, Berkovic SF, Steinlein OK, Bertrand D (1998) *Br J Pharmacol* 125:751–760.
15. Alkondon M, Pereira EF, Eisenberg HM, Albuquerque EX (2000) *J Neurosci* 20:66–75.
16. Porter JT, Cauli B, Tsuzuki K, Lambolez B, Rossier J, Audinat E (1999) *J Neurosci* 19:5228–5235.
17. Gourfinkel-An I, Baulac S, Nabbout R, Ruberg M, Baulac M, Brice A, LeGuern E (2004) *Lancet Neurol* 3:209–218.
18. Lambe EK, Picciotto MR, Aghajanian GK (2003) *Neuropsychopharmacology* 28:216–225.
19. Vidal C, Changeux JP (1993) *Neuroscience* 56:23–32.
20. Christophe E, Roebuck A, Staiger JF, Lavery DJ, Charpak S, Audinat E (2002) *J Neurophysiol* 88:1318–1327.
21. Dobelis P, Hutton S, Lu Y, Collins AC (2003) *J Pharmacol Exp Ther* 306:1159–1166.
22. Xiang Z, Huguenard JR, Prince DA (1998) *Science* 281:985–988.
23. Provini F, Plazzi G, Tinuper P, Vandi S, Lugaresi E, Montagna P (1999) *Brain* 122:1017–1031.
24. Herman ST, Walczak TS, Bazil CW (2001) *Neurology* 56:1453–1459.
25. Cobb SR, Buhl EH, Halasy K, Paulsen O, Somogyi P (1995) *Nature* 378:75–78.
26. Ji D, Dani JA (2000) *J Neurophysiol* 83:2682–2690.
27. Bandyopadhyay S, Sutor B, Hablitz JJ (2006) *J Neurophysiol* 95:1908–1916.
28. D'Antuono M, Louvel J, Kohling R, Mattia D, Bernasconi A, Olivier A, Turak B, Devaux A, Pumain R, Avoli M (2004) *Brain* 127:1626–1640.
29. Szabadics J, Varga C, Molnar G, Olah S, Barzo P, Tamas G (2006) *Science* 311:233–235.
30. Marty A, Llano I (2005) *Trends Neurosci* 28:284–289.